Silicon (2021) 13:2289–2307
https://doi.org/10.1007/s12633-020-00798-3

ORIGINAL PAPER

Radiation, Crystallization, and Physical Properties of Cadmium Borate Glasses

A.F. Abd El-Rehim [1,2] · H.Y. Zahran [1,2] · I.S. Yahia [1,2] · Sayed A. Makhlouf [3] · Kh. S. Shaaban [4]

Received: 27 September 2020 / Accepted: 20 October 2020 / Published online: 7 November 2020

Abstract
The melt-quenching method has been used to fabricate $Na_2B_4O_7$ - CdO glass system. The XRD diffractometer procedure was used to check the status of these samples. Inter-ionic distance (R_i) between Cd–Cd, Polaron radius r_p, and inter-nuclear distance r_i reduced with Cd content due to reducing molar volume. Ionicity I_b decreased and covalent glass character increased as CdO in the glass matrix increases. As the CdO contents increase, the values of T_g, T_c, and T_P have been increased. All expected phases are displayed in the XRD patterns. SEM has studied the morphology of the vitreous ceramic. It has been noted that the velocities and elastic modulus of glass-ceramics samples are increased. The structural nature of the developed phase was monitored in spectroscopic FT-IR investigations of the glass-ceramic samples. Mass attenuation Coefficient (μ/ρ) increases with CdO-content increase. The Z_{eff} values increase gradually at higher energy because of X-ray K-edges. Hence, the increase in CdO content can be developed the γ -radiation. According to our data, G7 is the best sample for shielding properties.

Keywords SEM · Mechanical · Glass-ceramics · Radiation

1 Introduction

Glass is a highly transparent, amorphous material and it is melting of an inorganic component without crystallization. High-performance borate glasses for various applications are used. These samples offer improved electrical conduction, glass formation, and temperature adjustment as compared to their binary system, which is the most suitable for solid-state batteries, low melting, and nonlinear optics [1–8].

Due to its easy performance, its higher density and gamma-ray attenuation coefficients are several applicable cadmium borate glasses. CdO is a heavy metal oxide (HMO), high density, and lower atomic radii [9–12]. Glasses of heavy metal oxide (HMO), includes about 50 mol of a heavy metal cation percent, (HMO) like CdO, MoO_3, Fe_2O_3, Bi_2O_3, Ga_2O_3, BaO, and PbO. These glasses have photon energy smaller than other glasses, and a higher refractive index. Therefore, the HMO glasses are transparent, promising materials for optoelectronics, fibers, sensors, optical instruments, good thermal, mechanical, and chemical stability, also offer superior optical and electrical properties [13, 14].

The recent development of cadmium borate glasses is very important scientifically and technologically. This importance comes from the structural factors associated with covalent links in the presence of CdO_4 structural units [15, 16]. CdO-B_2O_3 glasses can be used in numerous requests like laser hosts, nuclear protective, and neutron absorption. In recent years, glasses beside CdO & B_2O_3 have been studied extensively due to its interesting features, high dielectric, good infrared transmission, and low melting temperatures [17–19]. CdO glasses can be classified into Cd^{4+} and, Cd^{6+} structural investigations [17–19]. CdO is one of the significant oxide glass components. Further adding CdO to the glass enhances its mechanical strength, its chemical stability, and its thermal stability [19].

✉ Kh. S. Shaaban
khamies1078@yahoo.com

1 Physics Department, Faculty of Science, King Khalid University, P.O. Box 9004, Abha 61413, Saudi Arabia

2 Physics Department, Faculty of Education, Ain Shams University, P.O. Box 5101, Heliopolis 11771, Roxy, Cairo, Egypt

3 Physics Department, Faculty of Science, Assiut University, P.O. 71452, Assiut, Egypt

4 Chemistry Department, Faculty of Science, Al-Azhar University, P.O. 71452, Assiut, Egypt

Radiation has an enormous effect and applications in our everyday lives. In medicine, it can be used. Hazard impacts can be established by radiation discharge on living organisms [20, 21]. In several studies, the measurement of these doses has been analysed to achieve safe doses of exposure to radiation [12, 22–26]. Glass is one of the critical requirements that, because of its ease of preparation and high transparency, can be used to protect against the impact of harmful rays [12, 20–28].

In glass science and in glass technology, crystallization is an important subject. It is important to understand the crystallization mechanisms in the field of science and technology [30, 31]. This study aims to protect the glass system by crystallization, structural, mechanical, gamma, and neutron protection using Phy-X / PSD [29] of the cadmium borate glasses.

2 Experimental Procedures and Techniques

The x CdO - (100-x) $Na_2B_4O_7$ glasses [15] are summarized in Table 1 have been prepared in ceramic containers using a melting quenching method at 1000 °C and annealed at 450 °C, according to the chemical reaction [15]:

$$Na_2B_4O_7.10H_2O + CdO \xrightarrow[-(10H2O)]{\Delta} [Na_2B_4O_7 + CdO] \rightarrow^{\Delta\ 1000^{\circ}C} glasses \rightarrow^{annealing\ at\ 450^{\circ}C}$$

cadmium borate glass samples.

All chemicals used for the glass preparation obtained from Sigma-Aldrich. The XRD diffractometer procedure (PW/1710) was used to check the status of these glasses and glass-ceramics. DTA-50 Shimadzu used for the thermal investigation. By heating the specimen at specified temperatures two steps, first, at 500 °C, the glass-ceramics are produced. At 1 h at T_c °C, the other is crystal growth. In wave numbers 400–4000 cm^{-1}, at room temperature FTIR type JASCO – 430 used for measuring the FT-IR absorption spectrum of glass-ceramic. Mechanical measurements for glass-ceramics were studied by a pulse-echo technique, (KARL DEUTSCH Echograph model 1085). The type (JEM-100 CX 11 JAPAN), a scanning microscope (SEM), has been used to examine the morphology of glass-ceramics investigated.

3 Results and Discussion

3.1 Physical Properties

The XRD in Fig. 1 did not display sharp peaks, which indicate a high glass state of the glass samples.

The density of these glasses rises, and the molar volume reduces. The density increased because of the difference of density between $Na_2B_4O_7$ (2.46 g. cm^{3-}) and CdO (8.15 g. cm^{3-}). The decrease in molar volume because of the increase in density [7, 32–35].

Cd ion concentration was calculated as $Cdi = \left(\frac{6.023\times10^{23}x\ mol\ fraction\ of\ cation\times valency\ of\ cation}{Vm}\right)$. The concentration of Cd^{2+} is well known to increase because the molar volume decreases. Inter-ionic distance (R_i) was considered between two Cd^{2+}- Cd^{2+} as $R_i = \left(\frac{1}{\text{content of Cd}}\right)^{\frac{1}{3}}$, It is well known that with the Cd^{2+} concentration, R_i decreased in because of the molar volume decrease.

B – B separation ($d_{B\text{-}B}$) estimated as $(dB{-}B) = \left(\frac{V_m^B}{N}\right)^{\frac{1}{3}}$ and $V_m^B = \frac{Vm}{2(1-2Xn)}$. The ($d_{B\text{-}B}$) values have decreased as molar volume has decreased. Polaron radius r_p and inter-nuclear

Table 1 Chemical compositions (mol, %), weight fraction and mole fraction of the prepared glasses

Sample name	Chemical composition		Wi: Weight fraction of elements				Fi: Mole fraction of elements			
	$Na_2B_4O_7$	CdO	Na	B	O	Cd	Na	B	O	Cd
G 1	100	0	0.2285	0.2149	0.5566	0	0.1538	0.3077	0.5385	0
G 2	80	20	0.1971	0.1853	0.4971	0.1204	0.1481	0.2963	0.5370	0.0185
G 3	70	30	0.1794	0.1688	0.4638	0.1880	0.1443	0.2887	0.5361	0.0309
G 4	60	40	0.1603	0.1508	0.4277	0.2613	0.1395	0.2791	0.5349	0.0465
G 5	50	50	0.1395	0.1312	0.3883	0.3410	0.1333	0.2667	0.5333	0.0667
G 6	40	60	0.1167	0.1098	0.3453	0.4281	0.1250	0.2500	0.5313	0.0938
G 7	30	70	0.0918	0.0863	0.2982	0.5237	0.1132	0.2264	0.5283	0.1321

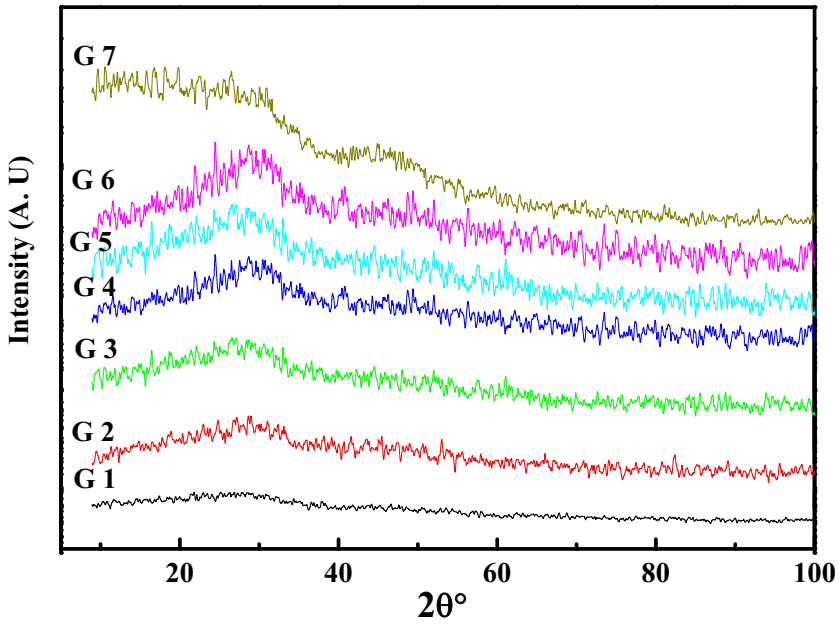

Fig. 1 XRD of the studied glasses

Table 2 Various physical parameters of the studied glasses

Samples	G 1	G 2	G 3	G 4	G 5	G 6	G 7
Number of oxygen atom	4.35	3.68	3.345	3.01	2.675	2.34	2.005
Avg. Mol. Wt. Mw (mol)	201.22	186.66	179.38	172.1	164.81	157.53	150.25
Density	2.307	2.662	2.863	3.294	3.67	3.98	4.25
Molar volume	87.22	70.12	62.65	52.25	44.91	39.58	35.35
Ion conc. (Tii) (10^{22} ions/cm^3)	–	0.688	1.16	1.85	2.69	3.66	2.05
Inter ionic Distance R_i (Å)	–	5.35	4.5	3.8	3.4	3.07	3.72
Inter-nuclear distance, ri (Å)	–	6.22	5.24	4.488	3.97	3.582	4.34
Polaron radius, r_p (Å)	–	1.78	1.5	1.29	1.14	1.03	1.245
B-B separation($d_{B\text{-}B}$) nm	0.75	0.65	0.6	0.53	0.48	0.43	0.37
oxygen packing density	49.87	52.48	53.39	57.6	59.56	59.12	56.7
(α cat)	6.967	6.155	5.75	5.34	4.94	4.53	4.13
Optical band gab (e.V)	3.25	3.16	3.01	2.73	2.35	2.31	2.26
Molar Refractivity theoretically	17.56	15.5	14.5	13.5	12.44	11.4	10.4
Basicity theoretically	1.665	1.663	1.662	1.66	1.659	1.657	1.655
Molar Refractivity, R_m(cm^3/mol)	52.06	42.25	38.35	32.9	29.5	26.13	23.47
Molar Polarizability, (A$^{\circ 3}$)	20.65	16.76	15.21	13.06	11.7	10.36	9.31
Reflection loss (R_L)	0.597	0.603	0.612	0.63	0.657	0.66	0.664
Metallization criterion (M)	0.403	0.397	0.388	0.37	0.343	0.34	0.336
Electronegativity (χ)	0.8736	0.849	0.809	0.73	0.632	0.621	0.607
Electron Polarizability (α°)	2.714	2.74	2.77	2.84	2.93	2.94	2.95
Optical basicity ( )	1.263	1.275	1.295	1.333	1.38	1.389	1.396
Average coordination number (m)	3.34	3.472	3.538	3.604	3.67	3.736	3.802
Number of bonds per unit volume nb (10^{29} m^{-3})	0.231	0.298	0.34	0.415	0.492	0.568	0.38
Ionicity (I_b)	0.542	0.54	0.539	0.5389	0.5382	0.5376	0.5369
Covalency (I_c)	0.458	0.46	0.461	0.4611	0.4618	0.4624	0.4631
($\wedge_{Th}$) Theoretically basicity	0.66	0.75	0.8	0.84	0.88	0.92	0.97
The two-photon absorption coefficient	10.44	11.16	12.38	14.65	17.725	18.05	18.45
packing density (Vi), $Vi \times 10^{-6}$, (m^3)	0.2	0.227	0.24	0.273	0.298	0.317	0.33
Dissociation energy (*Gi*), (kcal/kJ)	15.79	14.15	13.33	12.52	11.7	10.88	10.06

distance r_i were estimated as $rp = \frac{1}{2}\left(\frac{\pi}{6N}\right)^{\frac{1}{3}}$, $ri = \left(\frac{1}{N}\right)^{\frac{1}{3}}$. These parameters decrease because of the decrease in molar volume when CdO has increased.

Molar refractivity theoretically, and molar refractivity according to band gap $R_m = Vm\left(1-\sqrt{Eg/20}\right)$., molar polarizability $\propto_m = \left(\frac{3}{4\pi N}\right)R_m$, electronegativity (χ) $\chi = 0.2688E_{opt.}$, metallization $M = 1-\frac{R_m}{Vm}$ and basicity $\wedge = -0.5\chi + 1.7$have been estimated. It observed that due to an increase in CdO concentration these values were decreased [7, 32–35].

Reflection loss $R_L = \left(\frac{R_m}{Vm}\right)$, and polarization of the electron $\propto^{\circ} = -0.9\ \chi + 3.5$ are increased. These increases relate to molar volume decrease. Table 2 shows these values.

To confirm BO or NBO [36–38] connect, the coordinated average number is an important parameter [52–54]. The average number of coordinates (m) is calculated using the equation $m = \sum n_{ci}X_i$ where n_{ci} is the coordination of cation. It is found that the value of m is increased with CdO.

The volume of bonds per unit calculated by $n_b = \frac{N_A}{} V_m \sum n_{ci}X_i$ where N_A Avogadro constant. It is found that our results indicated n_b increases as the CdO content increases. It obviously shows modifying the role of CdO in samples with producing additional [BO_4].

The two-photon absorption (TPA) factor is one of the most important parameters for solid-state physics. TPA (β) cm /GW, it expressed as $\beta = 36.67 - 8.1E_g$, where E_g bandgap energy. It found that the TPA increases with the increase of CdO this increased connected to E_g. So, cadmium borate glasses may be used as a photonics application.

The ionic and covalent character of glasses can be determined. It estimated by electronegativity change of glass, $\Delta X = \sum X_i \Delta X_i$, *where* $\Delta X_i = X_O - X_M$, ionicity estimated as $I_b = [1-e^{(-0.25)}\ (X^2))\ ]$. It found that ionicity I_b decreases and covalent glass character increased as CdO in the glass network increases. In the semiconductor region, the conversion of covalent to ionic glass behaviors causes the $E_g$to decrease. Table 2 shows these values.

Table 3 Thermal parameter values of the studied glasses

Sample name	T_g (°C)	T_c	T_p
G 1	400	505	592
G 3	478	571	617
G 5	519	607	660
G 7	578	630	660

3.2 Thermal Analysis

When glass samples were heated at room temperature, there are several thermal changes. DTA-thermograms are the best way to show these things. The first thermal property is the transition of the glass T_g, while the next thermal property consists of T_c and T_p crystallization. These values are shown in Table 3. It is observed that these parameters

Table 4 XRD parameters of glass ceramic G1

Pos. [°2Th.]	Height [cts]	FWHM [°2Th.]	d-spacing [Å]	Rel. Int. [%]	Tip width [°2Th.]	G size nm	Matched by
7.0147	88.53	0.4723	12.6019	24.12	0.4800	59.3479	
14.5810	49.63	0.9446	6.07514	13.52	0.9600	29.8598	00-030-0199
19.2509	286.46	0.3542	4.61069	78.04	0.3600	80.1158	00-030-0199
20.4727	173.06	0.2952	4.33820	47.15	0.3000	96.3077	
21.0205	210.62	0.2952	4.22637	57.38	0.3000	96.3920	00-030-0199
27.1552	88.05	0.3542	3.28391	23.99	0.3600	81.258896	00-030-0199
27.9253	195.52	0.2952	3.19508	53.27	0.3000	97.660377	00-030-0199
30.0453	367.05	0.4723	2.97428	100.00	0.4800	61.332924	00-030-0199
32.1403	340.45	0.4723	2.78504	92.75	0.4800	61.645673	01-077-0210
33.8347	296.66	0.4133	2.64934	80.82	0.4200	70.754912	00-030-0199; 01-077-0210
36.1159	79.88	0.3542	2.48706	21.76	0.3600	83.080183	00-030-0199
43.3694	107.33	0.4723	2.08644	29.24	0.4800	63.748151	00-030-0199
47.6144	39.71	0.7085	1.90986	10.82	0.7200	43.161013	01-077-0210
49.6908	102.35	0.9446	1.83482	27.89	0.9600	32.639326	
53.3482	103.51	0.3542	1.71733	28.20	0.3600	88.395484	01-077-0210
54.8350	115.95	0.4320	1.67285	31.59	0.3600	72.9578	00-030-0199; 01-077-0210

Table 5 XRD parameters of glass ceramic G4

Pos. [°2Th.]	Height [cts]	FWHM [°2Th.]	d-spacing [Å]	Rel. Int. [%]	Tip width [°2Th.]	G size nm	Matched by
13.6527	41.41	0.3542	6.48606	6.29	0.3600	79.55189	00-030-0199
18.9946	158.73	0.4133	4.67232	24.12	0.4200	68.63377	00-030-0199
20.9488	130.94	0.4133	4.24068	19.90	0.4200	68.84017	00-030-0199
22.4569	164.81	0.4133	3.95918	25.05	0.4200	69.01406	00-030-0199
25.2588	148.62	0.4723	3.52600	22.59	0.4800	60.70557	00-030-0199
27.5511	658.00	0.5314	3.23761	100.00	0.5400	54.20796	00-030-0199
29.6129	548.29	0.4133	3.01673	83.33	0.4200	70.018	00-030-0199
30.9949	472.76	0.4133	2.88529	71.85	0.4200	70.24705	00-030-0199; 01-077-0210
31.7923	378.50	0.3542	2.81472	57.52	0.3600	82.12856	00-030-0199; 00-049-1842
33.0705	346.99	0.4723	2.70880	52.73	0.4800	61.7922	00-030-0199
34.0732	75.36	0.4133	2.63134	11.45	0.4200	70.79988	00-030-0199; 00-049-1842; 01-077-0210
37.5740	103.64	0.4133	2.39384	15.75	0.4200	71.50252	01-077-0210
38.7169	61.24	0.3542	2.32576	9.31	0.3600	83.72127	01-077-0210
44.5355	53.84	0.5904	2.03448	8.18	0.6000	51.20621	00-049-1842
45.9798	195.81	0.4723	1.97388	29.76	0.4800	64.34767	00-049-1842
48.2527	225.54	0.3542	1.88608	34.28	0.3600	86.54825	00-049-1842
53.1028	146.55	0.4133	1.72469	22.27	0.4200	75.6741	00-049-1842; 01-077-0210
53.9008	102.97	0.3542	1.70102	15.65	0.3600	88.61119	00-030-0199; 00-049-1842; 01-077-0210
59.7678	81.31	0.4723	1.54731	12.36	0.4800	68.32095	01-077-0210
71.7778	75.58	0.4723	1.31511	11.49	0.4800	73.11781	01-077-0210
77.9684	37.63	0.9446	1.22545	5.72	0.9600	38.10324	01-077-0210
80.3669	34.42	0.7085	1.19481	5.23	0.7200	51.68757	01-077-0210
83.1244	37.05	0.8640	1.16108	5.63	0.7200	43.27699	01-077-0210

have been increased as the CdO increases. These increases related to the increase in the packing density and to increase in the connection of the glass structure. According to these parameters, the glass-ceramics have been prepared.

3.3 XRD, SEM of Glass-Ceramics

Cadmium borate glass-ceramics are good resistance to chemical substances and offer great potential in a wide range of applications. During glass transformation in

Table 6 XRD parameters of glass ceramic G7

Pos. [°2Th.]	Height [cts]	FWHM [°2Th.]	d-spacing [Å]	Rel. Int. [%]	Tip width [°2Th.]	G size nm	Matched by
7.3390	80.80	0.5904	12.0457	10.62	0.6000	47.48477	00-030-0199
26.9638	732.71	0.3542	3.30679	96.33	0.3600	81.22624	00-030-0199
27.6676	760.61	0.3542	3.22425	100.00	0.3600	81.34756	00-030-0199
30.2255	334.44	0.2952	2.95696	43.97	0.3000	98.17008	00-030-0199
30.8823	301.39	0.2952	2.89556	39.62	0.3000	98.32388	00-030-0199
33.7688	279.18	0.3542	2.65436	36.71	0.3600	82.54629	00-030-0199; 00-049-1842; 01-077-0210
43.7886	207.37	0.3542	2.06744	27.26	0.3600	85.12793	00-049-1842; 01-077-0210
45.0945	108.43	0.3542	2.01056	14.26	0.3600	85.52518	00-049-1842; 01-077-0210
46.5194	290.82	0.4133	1.95224	38.23	0.4200	73.68154	00-030-0199; 00-049-1842
51.3551	87.06	0.3542	1.77920	11.45	0.3600	87.64296	00-049-1842
52.6809	126.99	0.5904	1.73750	16.70	0.6000	52.87751	00-049-1842
55.9818	149.55	0.5314	1.64263	19.66	0.5400	59.62333	00-030-0199
57.1831	191.81	0.4133	1.61094	25.22	0.4200	77.09442	01-077-0210
74.9099	57.36	0.5760	1.26665	7.54	0.4800	61.18689	01-077-0210

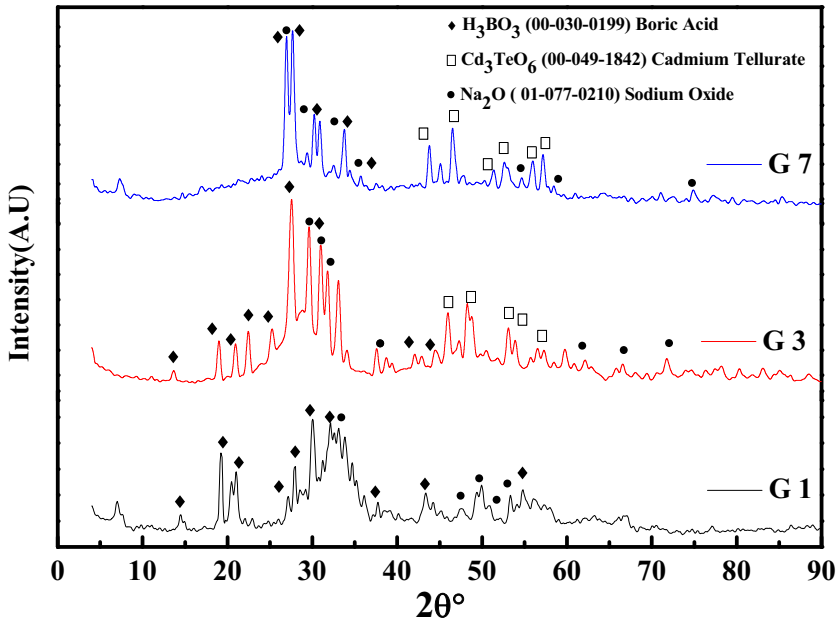

Fig. 2 XRD of the selected glass-ceramics

glass-ceramics, the structure and properties can be significantly changed [39–43]. Figure 2 demonstrations XRD of glass-ceramic samples. It was found that all phases expected appeared as boric acid H_3BO_3, card number (00-030-0199), sodium oxide Na_2O, card number (01-077-0210), and cadmium tellurate Cd_3TeO_6, card number (00-049-1842). Tables 4, 5 and 6 show the grain size of the phases and the matching phases by the X'Pert High Score program.

In Figs. 3 and 4 you can view SEM backscattered electron glass-ceramic images produced. The crystalline texture is observed contains comparatively bulky interstitial holes, showing the outstanding matrix of glass. This observation corresponds to the XRD analysis. The crystallinity and morphological properties of glass-ceramics had a direct effect on mechanical and chemical properties. The experiential morphological of the formed crystalline phases are found to differ including microcrystalline extended paths or fibrils, anhedral microcrystals, and a fine-grained texture. During thermal heat treatment, these different microcrystalline phases are associated with various precipitated sodium and boron phases. At the second stage of microcrystalline creation, cadmium tellurate phases are formed. Due to the

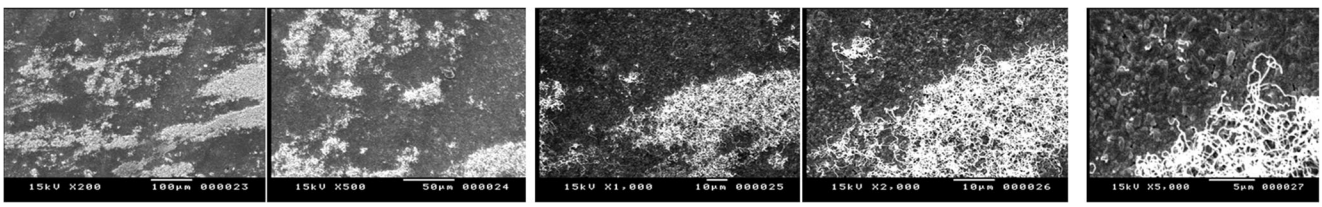

Fig. 3 SEM of G1 the selected glass -ceramics at magnifications 200, 500, 1000, 2000 and 5000

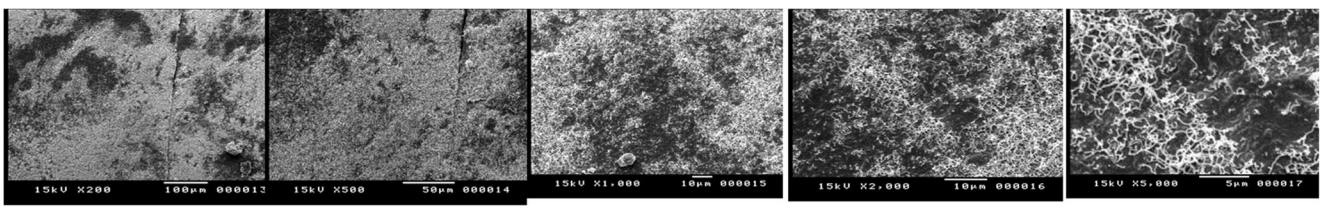

Fig. 4 SEM of G7 the selected glass -ceramics at magnifications 200, 500, 1000, 2000 and 5000

Table 7 The values of sound velocities, elastic moduli, micro-hardness (H), thermal expansion coefficient (α_P), acoustic impedance (Z) and density of the studied glass-ceramics

Sample name	V_L m/s	V_T	L	G (GPa)	K	Y	H	α_P, (K^{-1})	Zx10^7 ($kg.m^{-2}.s^{-1}$)	Density $g.cm^{3-}$
G 1	5025	2910	68.86	23.09	38.07	57.63	3.88	116,566.67	1.22	2.727
G 2	5205	2990	76.45	25.23	42.82	63.26	4.14	120,742.67	1.23	2.822
G 3	5310	3040	85.12	27.90	47.92	70.10	4.53	123,178.67	1.24	3.019
G 4	5420	3070	97.12	31.16	55.57	78.76	4.91	125,730.67	1.22	3.306
G 5	5465	3130	109.97	36.07	61.87	90.61	5.87	126,774.67	1.27	3.682
G 6	5515	3330	115.33	42.05	59.27	102.02	8.04	127,934.67	1.57	3.792
G 7	5715	3540	136.92	52.53	66.87	124.89	10.90	132,574.67	1.80	4.193

presence of different phases, crystals' dimensions of different habits ranged from 5 to 10 μm.

3.4 Mechanical Properties of the Glass-Ceramics

In comparison with the parent glasses, the density of the ceramics has increased. This growth is linked to heat treatment. I believe that heat treatment relieves the structure of glass by releasing some of its inner energy, causing a certain order and compactness. Different properties should therefore emerge, and the density should be increased.

In Fig. 5 you can view the velocities of prepared glass-ceramics (*VL*) and (*VT*). It was found that each velocity (*VL*, *VT*) is increased with the CdO increases these velocities are recorded in Table 7 [15]. *VL* arrange between 5025, 5715 m/s, and *VT* arrange between 2910, 3540 m/s. The increase in the velocities can be explaining by heat treatment relieves the structure of glass by releasing some of its inner energy, causing a certain order and compactness.

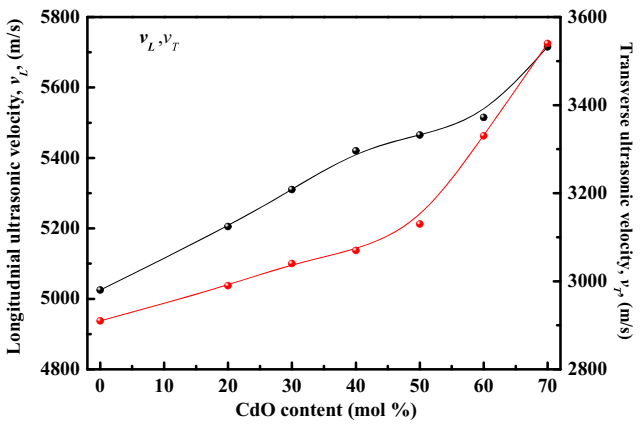

Fig. 5 Dependence of the longitudinal and shear ultrasonic velocities v_L and v_T of the investigated glass-ceramics with CdO content by mol %

In Fig. 6 you can view the elastic moduli of prepared glass-ceramics. It was found that the values of elastic modulus are increased. This increase can be explaining

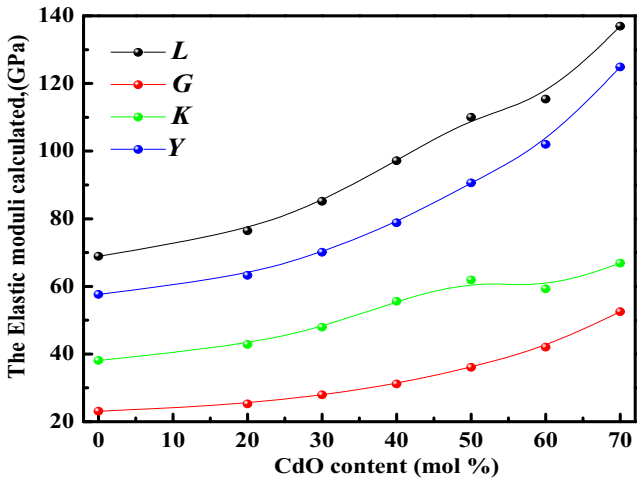

Fig. 6 Composition dependence of the elastic moduli of the studied glass-ceramics with CdO content by mol %

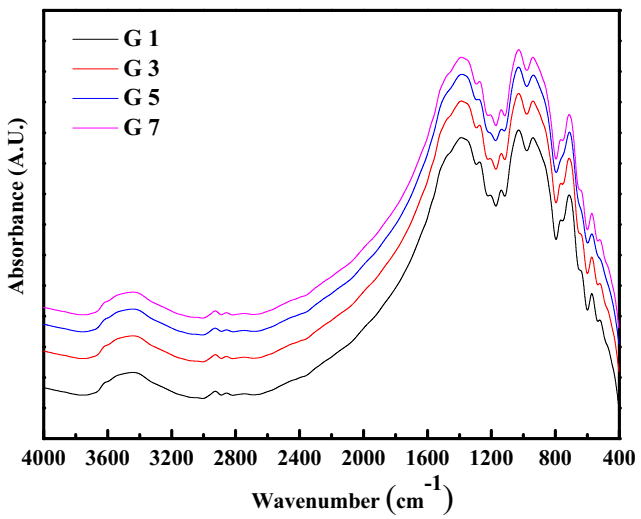

Fig. 7 Infrared spectra of the investigated glasses-ceramics

Table 8 De-convolution parameter of the infrared spectra of studied glasses (C) is the component band center and (A) is the relative area (%) of the component band

G 1	A	456	–	638	716	773	1151	1050	924	1259	1335	1457
	C	3.355	–	5.884	5.52	17.1	6.18	7.5	26	3	9.18	12.772
G 3	A	467.45	519	–	705	846	1139	1043	919	1266	1347	1485
	C	5.71	3.487	–	8.7	22.4	8.4	4.3	21.5	1.05	13.2	9.7
G 5	A	471.7	570	–	706	–	1124	1044	903	–	1368	1500
	C	7.931	5.2	–	12.43	–	17.5	4.67	28.2	–	13.95	9.1
G 7	A	459.56	572	621	712	772	1147	1048	919	1260	1358.8	1492
	C	3.264	6.22	8.34	6.85	14.15	5.5	7.7	26.9	3.99	15.83	7.44

by heat treatment relieves the structure of glass by releasing some of its inner energy, causing a certain order and compactness. Table 7 lists the density of glass ceramics, velocities, and elastic moduli of prepared glass-ceramics.

3.5 FT-IR Analysis for Glass-Ceramic

To verify the structural nature of the developed phase, the glass-ceramic investigations were applied by FT-IR [44, 45]. Figure 7 shows FT-IT measurements in the range 4000–400 cm^{-1} for glass-ceramic samples. Figure 8 displays the deconvolution of glass-ceramic samples in a region of 1600–400 cm^{-1}. Table 8 presents the de-convolution parameter of the FT-IR for preparation glass-ceramic. The bands ~1400, ~1274, ~1030, ~940, ~713, and ~ 574 cm^{-1} are reported by the FT-IT spectrum. The vibrations of the boroxol ring, B — O bond stretching of BO_3 units, and the bending vibrations of the B — O — B bridges are connected to the bands at 1400 and 1274 cm^{-1}. The vibration of boroxol, B — O bonding stretch of BO_4 units, and the bending vibration of B — O— B bridges are associated with bands at 1030 and 940 cm^{-1}. As we have observed, polycrystalline shows strong bands with FT-IR at ~713 and ~ 574 cm^{-1} described B — O—Cd, Na — O— Cd and Cd — O— Cd bending modes and CdO_4 tetrahedron.

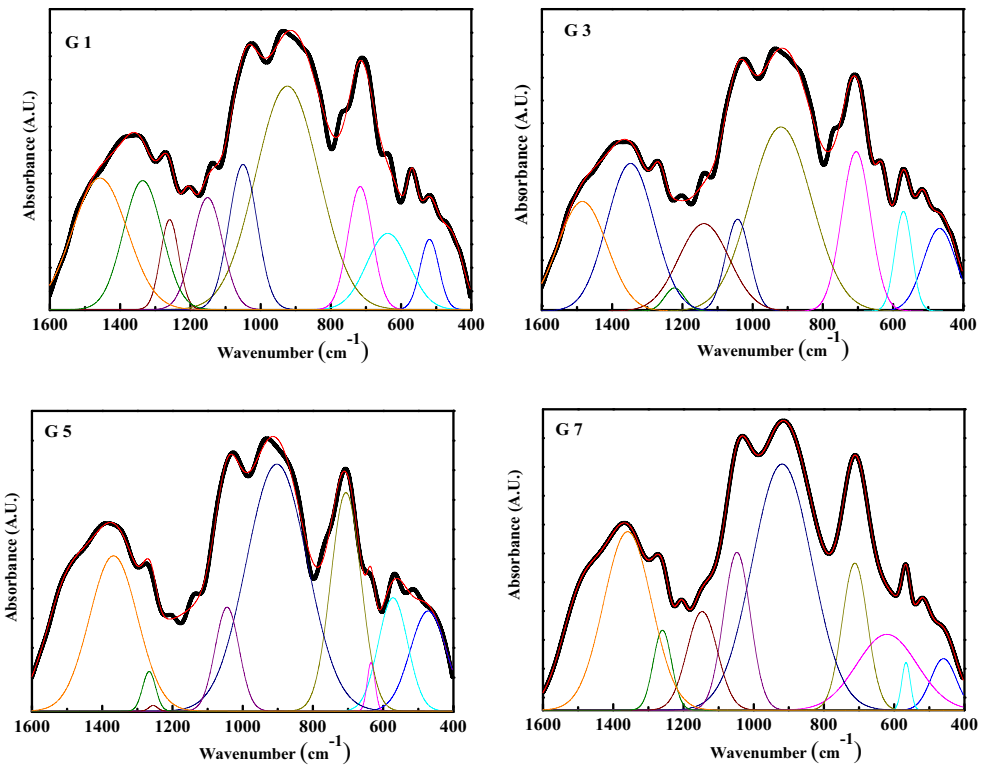

Fig. 8 Curve-fitting of FT-IR spectra of the glasses-ceramics samples

Table 9 Mass attenuation coefficients (cm^2/g) of prepared samples in comparison with different glass samples

Samples	MAC, (MeV)	
	0.02	10
G 7 [Present work]	10.529	0.030
$66B_2O_3$-$5Al_2O_3$-$29Na_2O$	1.074	0.020
$5Bi_2O_3$-$61B_2O_3$-$5Al_2O_3$-$29Na_2O$	5.059	0.022
$10Bi_2O_3$-$56B_2O_3$- $5Al_2O_3$-$29Na_2O$	9.043	0.023
0PbO-30SiO_2-46.67B_2O_3-23.33Na_2O	1.386	0.023
5PbO-25SiO_2-46.67B_2O_3-23.33Na_2O	5.167	0.021
10PbO-20SiO_2-46.67B_2O_3-23.33Na_2O	8.952	0.024
49.46SiO_2-26.38Na_2O- 23.08CaO- 1.07P_2O_5	3.982	0.024
47.84SiO_2-26.67Na_2O- 23.33CaO- 2.16P_2O_5	3.985	0.023
44.47SiO_2-27.26Na_2O- 23.85CaO- 4.42P_2O_5	4.057	0.024
40.96SiO_2-27.87Na_2O- 24.39CaO- 6.78P_2O_5	4.113	0.024
37.28SiO_2-28.52Na_2O- 24.95CaO- 9.25P_2O_5	4.061	0.024
48.98SiO_2-26.67Na_2O- 23.33CaO- 1.02P_2O_5	3.983	0.023
43.66SiO_2-28.12Na_2O- 24.60CaO- 3.62P_2O_5	4.100	0.024
38.14SiO_2-29.62Na_2O- 25.91CaO- 6.33P_2O_5	4.190	0.022
40.71SiO_2-28.91Na_2O- 25.31CaO-5.07 P_2O_5	4.131	0.022

3.6 Coefficient of Mass Attenuation (μ/ρ)

The (μ/ρ) of the samples is illustrated in Fig. 8 and calculated by $\left(\frac{\mu}{\rho}\right) = \sum_i w_i \left(\frac{\mu}{\rho}\right)_i$. The ($\mu/\rho$) of the samples is shown to increase at small energy. Figure 9 represented the (μ/ρ) as a function of the CdO concentrations. It indicated that the CdO-content increases (μ/ρ) increase. This increase is linked to density. So, the addition of CdO increases the attenuation rate of gamma-radiation for the samples being prepared. Table 9 shows the comparison of MAC of prepared samples with different glass samples.

3.7 (Z_{eff}) (N_{eff}) and Z_{eq} of Prepared Glasses

The effective atomic number (Z_{eff}) estimated as $Z_{eff} = \left(\frac{\sigma_a}{\sigma_e}\right)$ where (σ_a) the atomic cross-sections σ_a $\sigma_a = \sigma_m \frac{1}{\sum_i} n_i = \left(\frac{\mu}{\rho}\right)_{target} / N_A \sum_i \frac{w_i}{A_i}$, and σ_e the electronic cross-sections $\sigma_e = \frac{1}{N} \sum_i \left(\frac{\mu}{\rho}\right)_i f_i \frac{wA_i}{z_i}$. Figure 10 shows the Z_{eff} of the studied samples, which varied with γ-energy. Z_{eff} is suggested to have a higher value for these glasses with low energy due to the interaction of the photoelectric at this range. The Z_{eff} values increase gradually at higher energy because of X-ray *K*-edges. The glass name G 7 having a higher value of the Z_{eff}. So, the addition of CdO to glasses increase the γ -radiation attenuation rate for the samples.

Electron density (N_{eff}) has been estimated as $N_{eff} = N \frac{Z_{eff}}{\sum_i} F_i A_i$. Figure 11 represented the (N_{eff}) value of the samples against energy. It is observed that (N_{eff}) decreased at lower energy and then slowly increased. This decrease is due to the Compton scattering interaction. So, the increase of CdO can be developed the γ -radiation. The increase in (N_{eff}) is related to the pair creation.

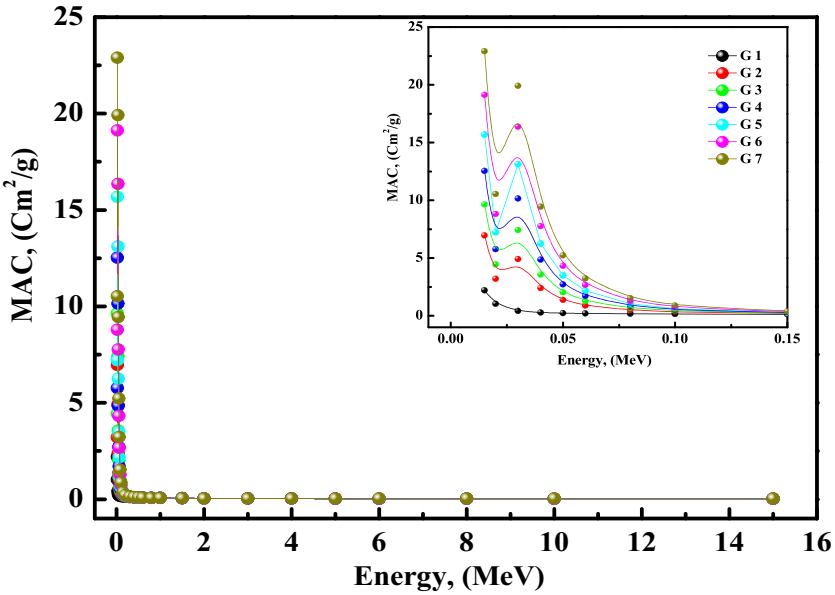

Fig. 9 The mass attenuation coefficient (μ/ρ) of prepared glasses

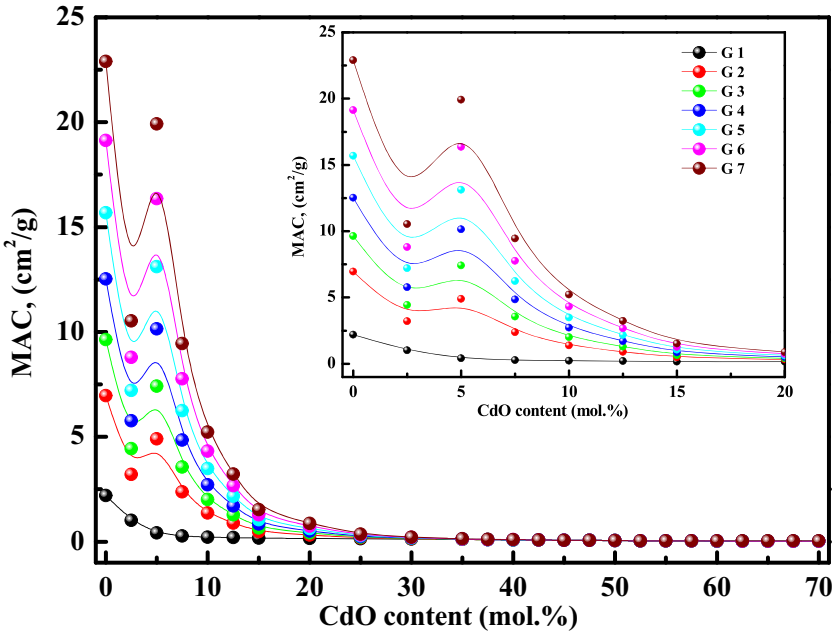

Fig. 10 The mass attenuation coefficient (μ/ρ) of the prepared glasses as a function of CdO content

Equivalent atomic number Z_{eq} can be estimated as $Zeq = \frac{Z1(\log R2-\log R)+Z2(\log R-\log R1)}{\log R2-\log R1}$. Figure 12 represented the (Z_{eq}) values of the samples between 0.015 and 15 MeV. It indicated that the (Z_{eq}) improved with the incident the photon energy and with the increase of CdO. The (Z_{eq}) value is increased with energy increased due to the Compton scattering interaction. For prepared samples, the highest (Z_{eq}) value at 1 MeV. At the higher energy than 1 MeV, the (Z_{eq}) value is decreased because of the pair creation interaction.

3.8 (HVL), (TVL) and, (MFP) of Prepared Glasses

The mean free path (MFP) was computed by $MEP = \left(\frac{1}{\mu}\right),$. It is possible to establish the tenth (TVL) and half-value

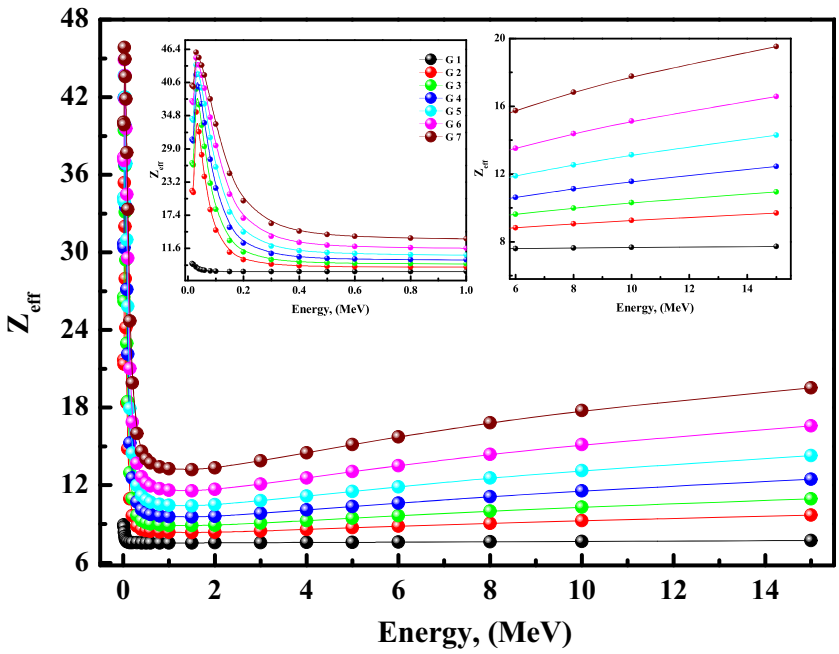

Fig. 11 The effective atomic number (Z_{eff}) of prepared glasses

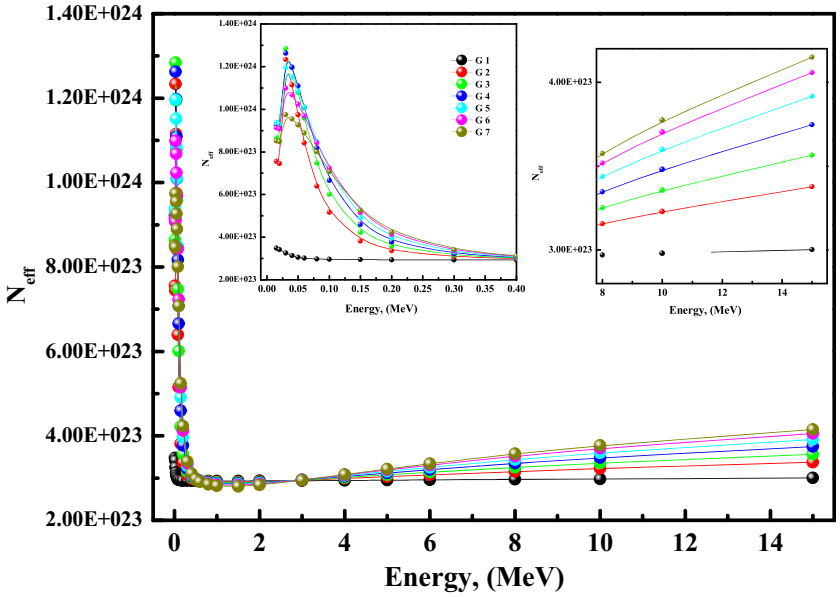

Fig. 12 The (N_{eff}) for the prepared glasses as a function of photon energy

layer (HVL) by $TVL = \left(\frac{\ln 10}{\mu}\right)$, $HVL = \left(\frac{\ln 2}{\mu}\right)$. Figures 13, 14 and 15 displays the (TVL), (HVL) and (MFP) values of the glasses. These parameter values are increased when photon energy is increased. This observation indicated that the increase in energy makes the photon allowed to intentionally transmit the sample. With the increase in CdO content, these values are decreasing. Therefore, CdO can enhance γ-radiation. According to our data, the best sample is G7. Figures 16 and 17 exemplified (HVL) and (MFP) comparisons of prepared samples to standard materials. These figures show that the lower value of (HVL) and (MFP) G7 are the better samples for γ radiation.

3.9 Exposure Construction of Glasses (EBF) and (EABF)

G–P fitting parameters have been estimated as $P = \frac{P1(\log Z2 - \log Zeq) + Z2(\log Zeq - \log Z1)}{\log Z2 - \log Z1}$. G–P fitting used for determined EABF and EBF, $B(E,X) = 1 + \frac{b-1}{K-1}(K^x - 1)$ for K≠1,

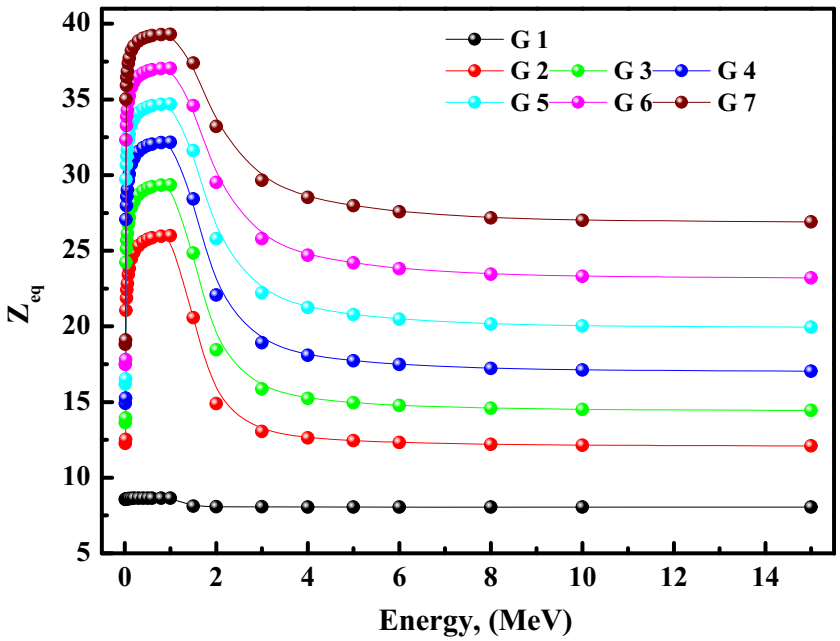

Fig. 13 Equivalent atomic number (Z_{eq}) for the prepared glasses as a function of photon energy

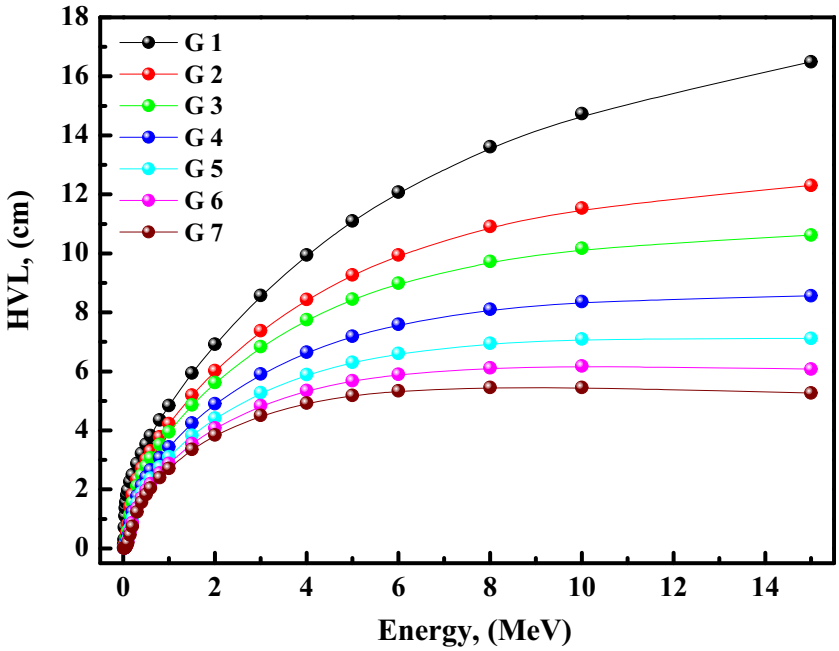

Fig. 14 The half value layer for the prepared glasses as a function of photon energy

$B(E, X) = 1 + (b - 1)x$ K=1 where $(E,X) = cx^a + d$ $\frac{tanh\left(\frac{x}{Xk}-2\right)-tanh(-2)}{1-tanh\ (-2)}$. Figures 18 and 19, and Tables 10 and 11. represented the (EBF) and, EABF of the samples [11, 46]. EBF and EABF values are low at the lower energy due to the glasses will absorb the energy photons then increased with the increase of energy due to Compton scattering. After that, decrease with increasing energy due to the pair production. In our study, Maximum radiation occurs at the sample surface. This means that prepared glasses have better shielding characteristics than those of the above standard shields. Besides, the CdO content of studied glasses should be improved so that similar protection properties such as G 7 glass can be achieved.

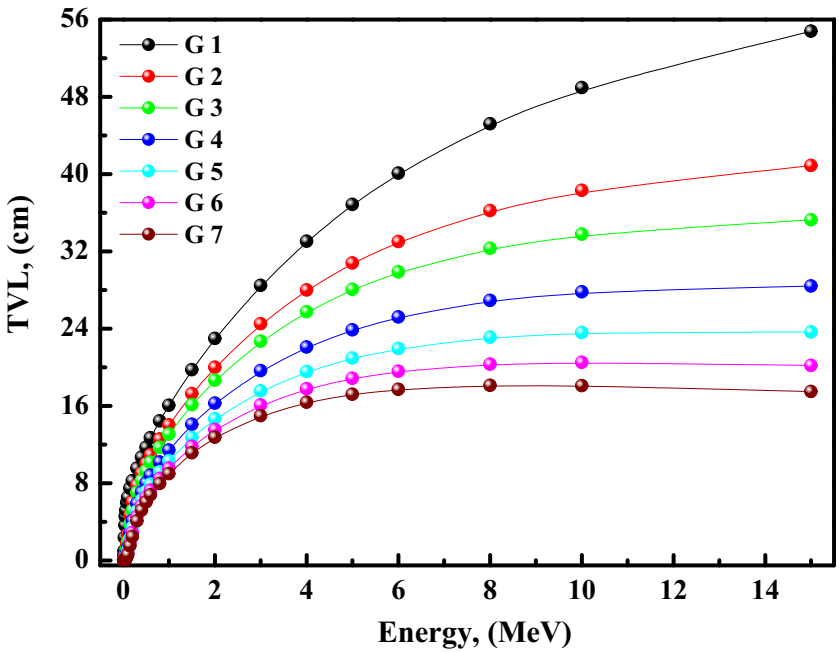

Fig. 15 The tenth value layer for the prepared glasses as a function of photon energy

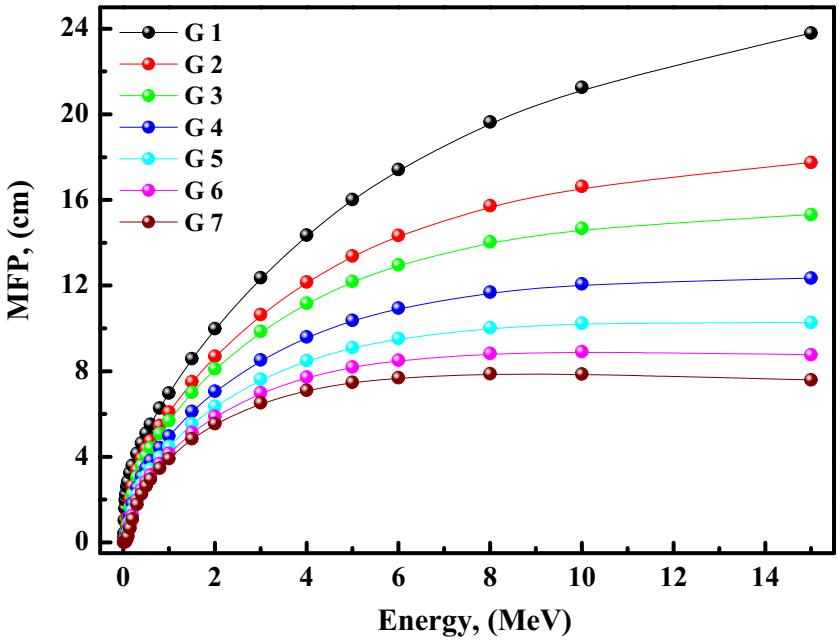

Fig. 16 The MFP for the prepared glasses as a function of photon energy

3.10 Fast Neutron Removal Cross-Section (FNRCS) (1/Cm)

Effective removal cross-section (Σ_R), can be estimated: $\left(\frac{\Sigma_R}{\rho}\right) = \sum_i w_i \left(\frac{\Sigma_R}{\rho}\right)_i$ and $R = \sum_i \rho_i \left(\frac{R}{\rho}\right)_i$. Figure 20 represented the (ΣR) of glass samples against the gamma energy. It is observed that the (ΣR) increased at lower energy. At higher energy, small deviations are observed of the glass samples decreasing the value of (ΣR). These small deviations in the results are related to the increase of CdO. The elements which have a light atomic number are well known to have a strong ability to shield the neutrons. Therefore, the increase in the content of CdO can lead to an improvement in the neutron's shielding. The increase of CdO enhances the ΣR

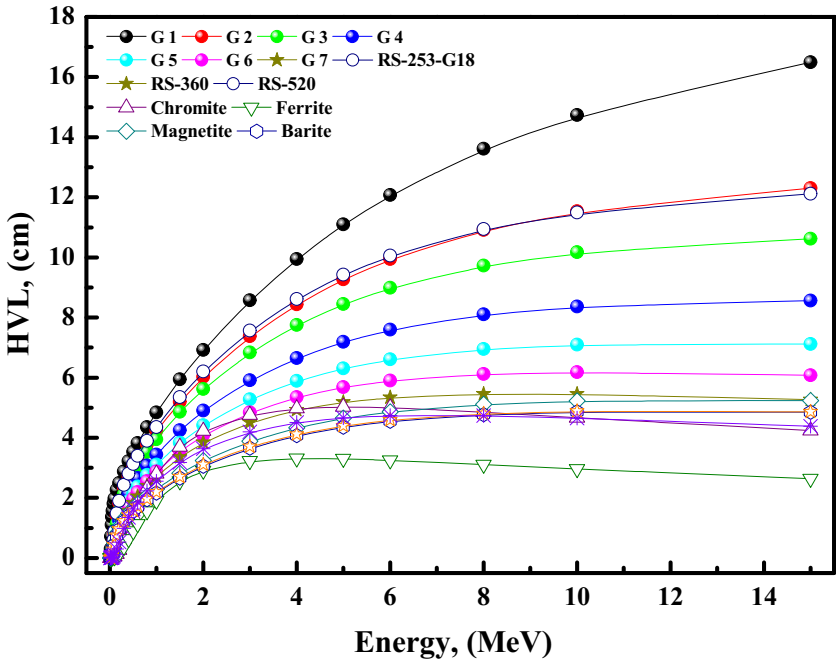

Fig. 17 The comparison of half value layer for the prepared glasses as a function of photon energy with standard materials

Table 10 G-P fitting parameters for EBF, and G-P fitting parameters for EABF of glass name G 1

Energy (MeV)	G-P Fitting Parameters for EBF					G -P Fitting Parameters for EABF				
	a	b	c	d	Xk	a	b	c	d	Xk
1.50E-02	0.196	1.132	0.421	−0.100	13.899	0.198	1.132	0.422	−0.101	12.789
2.00E-02	0.173	1.305	0.482	−0.089	14.411	0.172	1.309	0.482	−0.090	14.487
3.00E-02	0.106	1.907	0.665	−0.056	15.979	0.130	2.002	0.616	−0.057	12.236
4.00E-02	0.031	2.834	0.917	−0.021	14.111	0.035	2.913	0.909	−0.024	13.887
5.00E-02	−0.024	3.687	1.178	0.002	13.713	−0.025	3.800	1.183	0.002	13.764
6.00E-02	−0.069	4.206	1.414	0.024	13.641	−0.072	4.382	1.428	0.027	13.834
8.00E-02	−0.119	4.441	1.725	0.049	13.693	−0.124	4.764	1.752	0.053	13.237
1.00E-01	−0.140	4.234	1.885	0.058	13.967	−0.149	4.600	1.933	0.065	13.628
1.50E-01	−0.147	3.714	1.952	0.055	14.534	−0.159	3.950	2.026	0.064	14.194
2.00E-01	−0.153	3.236	1.979	0.058	14.174	−0.164	3.425	2.044	0.066	13.932
3.00E-01	−0.142	2.819	1.872	0.052	14.181	−0.151	2.931	1.924	0.059	14.044
4.00E-01	−0.131	2.593	1.769	0.048	14.409	−0.139	2.667	1.811	0.054	14.105
5.00E-01	−0.121	2.444	1.680	0.044	14.361	−0.128	2.493	1.719	0.050	14.273
6.00E-01	−0.110	2.335	1.601	0.040	14.589	−0.116	2.376	1.635	0.045	14.371
8.00E-01	−0.097	2.168	1.505	0.038	14.471	−0.098	2.217	1.507	0.038	14.498
1.00E+00	−0.081	2.080	1.403	0.031	14.681	−0.084	2.106	1.417	0.033	14.359
1.50E+00	−0.057	1.927	1.264	0.023	14.484	−0.056	1.943	1.261	0.022	14.309
2.00E+00	−0.036	1.836	1.164	0.014	15.371	−0.037	1.839	1.167	0.014	14.624
3.00E+00	−0.011	1.710	1.052	0.002	12.819	−0.011	1.710	1.052	0.002	14.266
4.00E+00	0.004	1.624	0.990	−0.007	20.302	0.006	1.621	0.986	−0.007	12.975
5.00E+00	0.016	1.553	0.947	−0.011	14.439	0.018	1.556	0.942	−0.013	13.265
6.00E+00	0.025	1.505	0.917	−0.023	15.541	0.029	1.505	0.907	−0.026	15.101
8.00E+00	0.033	1.417	0.891	−0.020	12.329	0.031	1.410	0.896	−0.017	12.329
1.00E+01	0.039	1.358	0.872	−0.025	13.971	0.041	1.355	0.868	−0.027	13.901
1.50E+01	0.050	1.265	0.842	−0.039	15.014	0.048	1.258	0.849	−0.036	14.749

values; therefore, we can say that the addition of CdO to glasses improves the γ -radiation attenuation [11, 46].

Figures 21 and 22 show the FNRCS of the prepared glasses. It was observed that the FNRCS values are increased as the CdO content increased. The increase in FNRCS is affected by glass composition and density. Therefore, we can say that the addition of CdO to glasses increase the FNRCS.

4 Conclusions

The Melt-quenching method has been used to fabricate $Na_2B_4O_7$ - CdO glass system. The XRD diffractometer procedure was used to check the status of these samples. The obtaining physical and optical values of $Na_2B_4O_7$ - CdO glass system can develop solid-state devices and optical memory equipment. Inter-ionic distance (R_i) between Cd–Cd, Polaron radius r_p, and internuclear distance r_i reduced with Cd content due to reducing molar volume. The volume of bonds per unit increases as CdO content. It obviously shows modifying the role of CdO in samples with producing additional BO_4. TPA increases with the increase of CdO this increased connected to E_g. So, $Na_2B_4O_7$ - CdO glasses may be used as a photonic-applications. Ionicity I_b decreased and covalent glass character increased as CdO in the glass matrix increases. As the CdO contents increase, the values of T_g, T_c, and T_P have been increased. All expected phases are displayed in the XRD patterns. SEM has studied the morphology of the vitreous ceramic. It has been noted that the velocities and elastic modulus of glass-ceramics samples are increased. The structural nature of the developed phase was monitored in spectroscopic FT-IR investigations of the glass-ceramic samples. It indicated that the CdO-content increases (μ/ρ) increase. The Z_{eff} values increase gradually at higher energy because of X-ray K-edges. It is observed that (N_{eff}) decreased at lower energy and then slowly increased. As well as the (HVL), (TVL) and, (MFP) values decrease with the increase in CdO

Table 11 G-P fitting parameters for EBF, and G-P fitting parameters for EABF of glass name G 7

Energy (MeV)	G-P Fitting Parameters for EBF					G -P Fitting Parameters for EABF				
	a	b	c	d	Xk	a	b	c	d	Xk
1.50E-02	0.536	1.011	0.194	−0.558	14.555	0.373	1.010	0.272	−0.409	15.873
2.00E-02	0.277	1.023	0.305	−0.139	12.221	0.352	1.022	0.261	−0.245	12.270
3.00E-02	0.156	2.352	0.732	−0.136	22.235	0.175	1.270	0.741	−0.148	19.772
4.00E-02	0.152	2.717	0.325	−0.059	19.605	0.145	1.299	0.350	−0.148	24.161
5.00E-02	−0.104	2.333	0.158	−0.019	12.314	−0.003	1.264	0.167	0.022	10.048
6.00E-02	0.798	1.950	0.131	−0.143	16.118	0.606	1.254	0.135	−0.177	14.776
8.00E-02	0.586	1.512	0.163	−0.210	14.265	0.461	1.283	0.180	−0.195	14.150
1.00E-01	0.254	1.195	0.360	−0.137	13.791	0.271	1.248	0.336	−0.145	15.426
1.50E-01	0.155	1.311	0.537	−0.081	14.311	0.267	1.618	0.359	−0.154	13.950
2.00E-01	0.145	1.526	0.589	−0.085	14.134	0.272	2.355	0.392	−0.174	13.895
3.00E-01	0.064	1.647	0.794	−0.038	14.073	0.134	2.500	0.635	−0.087	13.795
4.00E-01	0.027	1.750	0.939	−0.029	13.644	0.085	2.701	0.784	−0.076	13.571
5.00E-01	0.007	1.799	1.018	−0.021	13.492	0.050	2.680	0.892	−0.056	13.455
6.00E-01	−0.003	1.813	1.060	−0.017	12.937	0.033	2.620	0.947	−0.046	13.200
8.00E-01	−0.013	1.812	1.101	−0.013	12.759	0.015	2.462	1.010	−0.035	12.781
1.00E+00	−0.017	1.790	1.112	−0.010	12.363	0.005	2.326	1.039	−0.027	12.400
1.50E+00	−0.032	1.658	1.169	0.004	10.652	−0.015	1.944	1.111	−0.013	11.811
2.00E+00	−0.021	1.661	1.123	−0.005	10.261	−0.011	1.840	1.089	−0.012	10.800
3.00E+00	−0.004	1.613	1.059	−0.015	12.248	0.003	1.676	1.036	−0.020	12.327
4.00E+00	0.008	1.547	1.023	−0.025	12.922	0.011	1.546	1.013	−0.029	14.060
5.00E+00	0.014	1.480	1.008	−0.029	13.214	0.021	1.459	0.985	−0.038	14.147
6.00E+00	0.022	1.434	0.988	−0.036	13.295	0.023	1.387	0.981	−0.039	14.314
8.00E+00	0.033	1.354	0.968	−0.047	13.589	0.034	1.295	0.958	−0.047	14.020
1.00E+01	0.042	1.294	0.953	−0.057	13.949	0.038	1.232	0.958	−0.050	14.291
1.50E+01	0.050	1.196	0.961	−0.061	14.405	0.050	1.146	0.952	−0.057	14.687

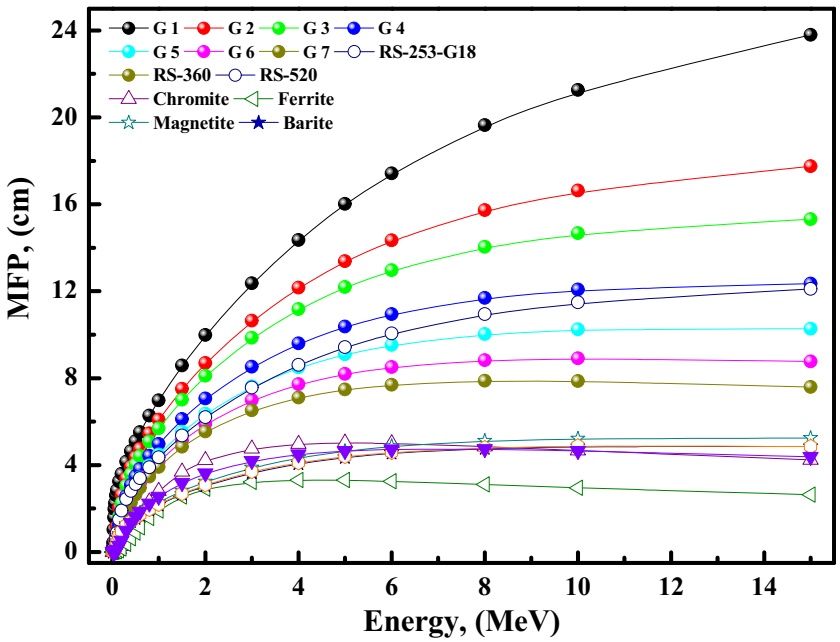

Fig. 18 The comparison of MFP for the prepared glasses as a function of photon energy with standard materials

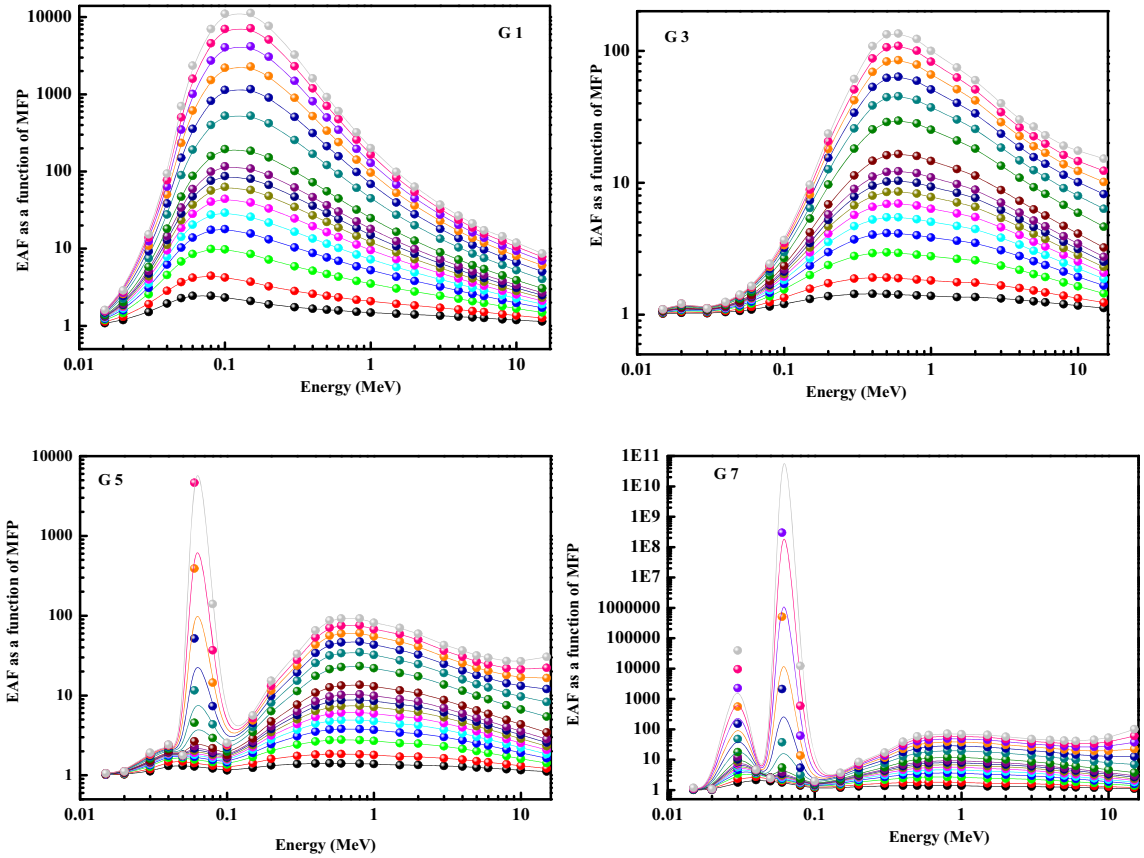

Fig. 19 Variation of EBF versus the gamma ray energy for Some prepared glasses as a function of photon energy

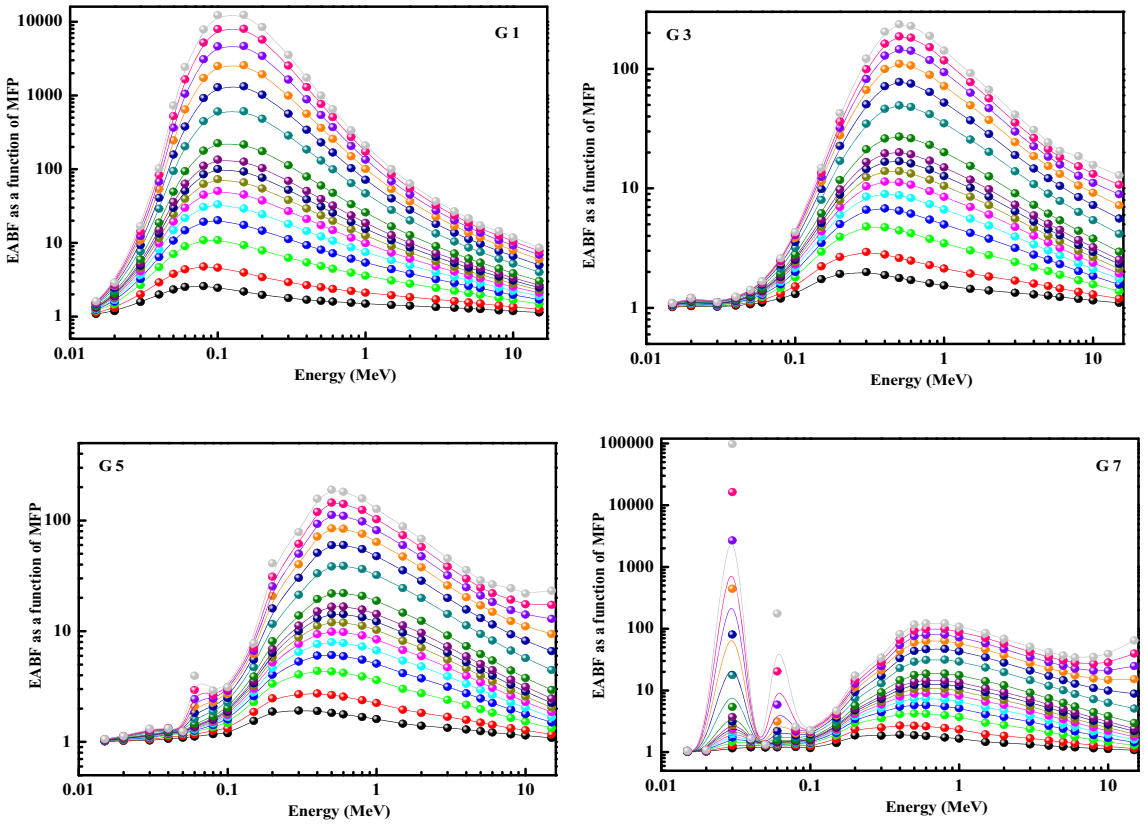

Fig. 20 Variation of EABF versus the gamma ray energy for the prepared glasses as a function of photon energy

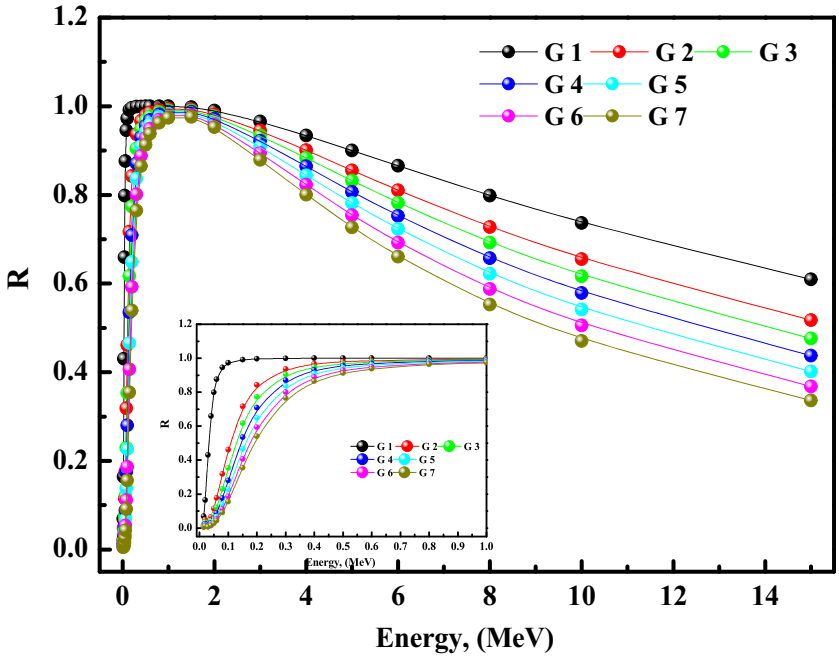

Fig. 21 Effective removal cross-through (ΣR) for the prepared glasses as a function of photon energy

content. Hence, the increase in CdO content can be developed the γ -radiation. EBF and EABF values are low at the lower energy due to the glasses will absorb the energy photons then increased with the increase of energy due to Compton scattering. It was observed that the FNRCS values are increased as the CdO content increased. According to our data, G7 is the best sample for shielding properties.

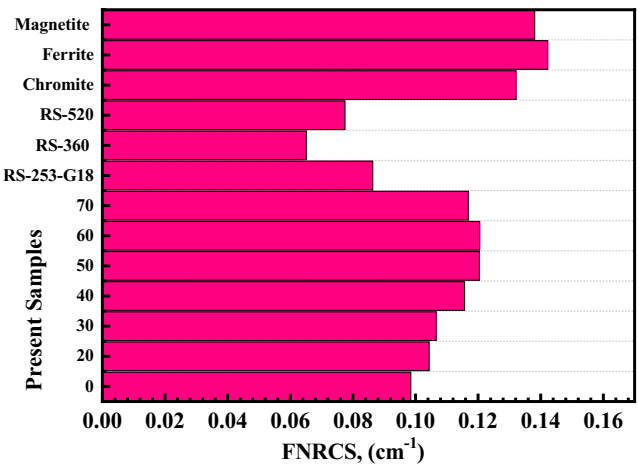

Fig. 22 FNRCS for the prepared glasses comparison with standard materials

Acknowledgments The authors extend their appreciation to the Deanship of Scientific Research at King Khalid University for funding this work through research groups program under grant number R.G.P. 2/93/41.

Compliance with Ethical Standards

Conflict of Interest authors declare that they have no conflict of interest.

Ethical Approval This article does not contain any studies with human participants or animals performed by any of the authors.

Informed Consent was obtained from all individual participants included in the study.

Declaration of Interests the authors declare that they have no known competing financial interests or personal relationships that could have appeared to influence the work reported in this paper.

References

1. Abd-Allah WM, Saudi HA, Shaaban KS, Farroh HA (2019) Investigation of structural and radiation shielding properties of $40B_2O_3$–30PbO–(30-*x*) BaO-*x* ZnO glass system. Appl Phys A Mater Sci Process 125:275. https://doi.org/10.1007/s00339-019-2574-0
2. Saudi HA, Abd-Allah WM, Shaaban KS (2020) Investigation of gamma and neutron shielding parameters for borosilicate glasses doped europium oxide for the immobilization of radioactive waste. J Mater Sci Mater Electron 31:6963–6976. https://doi.org/10.1007/s10854-020-03261-6
3. Shaaban K, Abdel Wahab EA, El-Maaref AA et al (2020) Judd–Ofelt analysis and physical properties of erbium modified cadmium

lithium gadolinium silicate glasses. J Mater Sci Mater Electron 31: 4986–4996. https://doi.org/10.1007/s10854-020-03065-8
4. Shaaban KS, Koubisy MSI, Zahran HY, Yahia IS (2020) Spectroscopic properties, electronic Polarizability, and optical basicity of titanium–cadmium Tellurite glasses doped with different amounts of lanthanum. J Inorg Organomet Polym. https://doi.org/10.1007/s10904-020-01640-4
5. Somaily HH, Shaaban KS, Makhlouf SA, Algarni H, Hegazy HH, Wahab EAA, Shaaban ER (2020) Comparative studies on polarizability, optical basicity and optical properties of lead borosilicate modified with titania. J Inorg Organomet Polym. https://doi.org/10.1007/s10904-020-01650-2
6. Shaaban KS, Yousef ES (2020) Optical properties of Bi_2O_3 doped borotellurite glasses and glass-ceramics. Optik - International Journal for Light and Electron Optics 203:163976. https://doi.org/10.1016/j.ijleo.2019.163976
7. Wahab EAA, Shaaban KS (2018) Effects of SnO_2 on spectroscopic properties of borosilicate glasses before and after plasma treatment and its mechanical properties. Materials Research Express 5(2): 025207. https://doi.org/10.1088/2053-1591/aaaee8
8. El-Sharkawy RM, Shaaban KS, Elsaman R, Allam EA, El-Taher A, Mahmoud ME (2020) Investigation of mechanical and radiation shielding characteristics of novel glass systems with the composition xNiO-20ZnO-60B_2O_3-(20-x) CdO based on nano metal oxides. J Non-Cryst Solids 528:119754. https://doi.org/10.1016/j.jnoncrysol.2020
9. Abdel Wahab EA, Shaaban KS, Elsaman R et al (2019) Radiation shielding, and physical properties of lead borate glass doped ZrO_2 nanoparticles. Appl Phys A 125(12):869. https://doi.org/10.1007/s00339-019-3166-8
10. Sharma V, Pal SS, Mudahar SG, Singh Thind K (2012) Synthesis and characterization of cadmium containing sodium borate glasses. New Journal of Glass and Ceramics 2:150–155. https://doi.org/10.4236/njgc.2012.24022
11. Kaur P, Singh D, Singh T (2016) Heavy metal oxide glasses as gamma rays shielding material. Nucl Eng Des 307:364–376 https://doi.org/10.1016/j.nucengdes.2016.07.029
12. Tekin HO, Kavaz E, Papachristodoulou A, Kamislioglu MO, Agar EE, Guclu A, Kilicoglu O, Sayyed MI (2019) Characterization of SiO_2–PbO–CdO–Ga_2O_3 glasses for comprehensive nuclear shielding performance: alpha, proton, gamma, neutron radiation. Ceram Int 45(15):19206–19222. https://doi.org/10.1016/j.ceramint.2019.06.168
13. Lezal D, Pedlikova J, Kostka P, Bludska J, Poulain M, Zavadil J (2001) Heavy metal oxide glasses: preparation and physical properties. J Non-Cryst Solids 284(1–3):288–295. https://doi.org/10.1016/S0022-3093(01)00425-2
14. Dumbaugh WH, Lapp JC (1992) Heavy-metal oxide glasses. J Am Ceram Soc 75(9):2315–2326. https://doi.org/10.1111/j.1151-2916.1992.tb05581.x
15. Saddeek YB, Aly KA, Shaaban KS, Mossad AA, Sayed MA (2018) Elastic, optical and structural features of wide range of CdO- Na2B4O7 glasses. Mater Res Express 5(6):065204. https://doi.org/10.1088/2053-1591/aac93f
16. Doweidar H, El-Damrawi G, El-Stohy S (2017) Structure and properties of CdO–B_2O_3 and CdO–MnO–B_2O_3 glasses; criteria of getting the fraction of four coordinated boron atoms from infrared spectra. Physica B 525:137–143. https://doi.org/10.1016/j.physb.2017.09.019
17. Sharma V, Pal SS, Singh MG, Singh TK (2012) Synthesis and characterization of cadmium containing sodium borate glasses. New Journal of Glass and Ceramics 2:150,150–150,155. https://doi.org/10.4236/njgc.2012.24022
18. Mohan S, Singh DP, Simranpreet K (2015) Structural and optical investigations of CdO-Na2CO3-H3BO3 glasses. Canadian Journal of Physics 93(7):796–801. https://doi.org/10.1139/cjp-2014-0404
19. Khamaganova TN, Khumaeva TG, Subanakov AK, Perevalov AV (2017) Synthesis and thermoluminescence properties of CdB_4O_7:Tb^{3+} and CdB_4O_7:Mn^{2+}. Inorg Mater 53:81–85. https://doi.org/10.1134/S0020168517010101
20. Møller AP, Mousseau TA (2013) The effects of natural variation in backgroundradioactivity on humans, animals and other organisms. Biol Rev 88:226–254. https://doi.org/10.1111/j.1469-185X.2012.00249.x
21. Mettler Jr FA, Huda W, Yoshizumi TT, Mahesh M (2008) Effective doses in radiology and diagnostic nuclear medicine: a catalog. Radiology 248:254–263. https://doi.org/10.1148/radiol.2481071451
22. Nowak M, Sans-Merce M, Lemesre C, Elmiger R, Damet J (2019) Eye lens monitoring programme for medical staff involved in fluoroscopy guided interventional procedures in Switzerland. Phys Med 57:33–40. https://doi.org/10.1016/j.ejmp.2018.12.001
23. König A, Etzel R, Thomas R, Mahnken A (2019) Personal radiation protection and corresponding dosimetry in interventional radiology: an overview and future developments. RöFo - Fortschritte Auf Dem Gebiet Der Röntgenstrahlen Und Der Bildgebenden Verfahren 191(06):512–521. https://doi.org/10.1055/a-0800-0113
24. Kosaka H, Monzen H, Matsumoto K, Tamura M, Nishimura Y (2019) Reduction of operator hand exposure in interventional radiology with a novel finger sack using tungsten-containing rubber. Health Phys 116(5):625–630. https://doi.org/10.1097/HP.0000000000000992
25. Etzel R, König AM, Keil B, Fiebich M, Mahnken AH (2018) Effectiveness of a new radiation protection system in the interventional radiology setting. Eur J Radiol 106:56–61. https://doi.org/10.1016/j.ejrad.2018.07.006
26. Chida K, Kaga Y, Haga Y, Kataoka N, Kumasaka E, Meguro T, Zuguchi M (2013) Occupational dose in interventional radiology procedures. Am J Roentgenol 200(1):138–141. https://doi.org/10.2214/AJR.11.8455
27. Kavaz E, Tekin HO, Agar O, Altunsoy EE, Kilicoglu O, Kamislioglu M, Abuzaid MM, Sayyed MI (2019) The mass stopping power/projected range and nuclear shielding behaviors of barium bismuth borate glasses and influence of cerium oxide. Ceram Int 45(12,15):15348–15357. https://doi.org/10.1016/j.ceramint.2019.05.028
28. Kalnins CAG, Ebendorff-Heidepriem H, Spooner NA, Monro TM (2016) Enhanced radiation dosimetry of fluoride phosphate glass optical fbres by terbium (III) doping. Opt Mater Express 6(12): 3692–3703. https://doi.org/10.1364/OME.6.003692
29. Şakar E, Özpolat ÖF, Alım B, Sayyed MI, Kurudirek M (2020) PhyX / PSD: Development of a user friendly online software for calculation of parameters relevant to radiation shielding and dosimetry. Radiation Physics and Chemistry 166:108496. https://doi.org/10.1016/j.radphyschem.2019.108496
30. Shaaban KS, Abo-Naf SM, Hassouna MEM (2019) Physical and structural properties of Lithium borate glasses containing MoO_3. Silicon 11:2421–2428. https://doi.org/10.1007/s12633-016-9519-4
31. Shaaban KS, Abo-naf SM, Abd Elnaeim AM, Hassouna MEM (2017) Studying effect of MoO3 on elastic and crystallization behavior of lithium diborate glasses. Applied Physics A 123(6):457. https://doi.org/10.1007/s00339-017-1052-9
32. Shaaban KS, Yousef ES, Mahmoud SA, Wahab EAA, Shaaban ER (2020) Mechanical, structural, and crystallization properties in Titanate doped phosphate glasses. J Inorg Organomet Polym 30: 4655–4663. https://doi.org/10.1007/s10904-020-01574-x
33. Shaaban KS, Wahab EAA, Shaaban ER, Yousef ES, Mahmoud SA (2020) Electronic polarizability, optical basicity, and mechanical properties of aluminum lead phosphate glasses. Opt Quant Electron 52:125. https://doi.org/10.1007/s11082-020-2191-3
34. Fayad AM, Shaaban KS, Abd-Allah WM, Ouis M (2020) Structural and optical study of CoO doping in Borophosphate host

glass and effect of gamma irradiation. J Inorg Organomet Polym. https://doi.org/10.1007/s10904-020-01641-3

35. Shaaban KS, Wahab EAA, Shaaban ER, Yousef ES, Mahmoud SA (2020) Electronic Polarizability, optical basicity, thermal, mechanical and optical investigations of ($65B_2O_3$–$30Li_2O$–$5Al_2O_3$) glasses doped with Titanate. Journal of Elec Materi 49:2040–2049. https://doi.org/10.1007/s11664-019-07889-x
36. Ibrahim S, Gomaa MM, Darwish H (2014) Influence of Fe_2O_3 on the physical, structural and electrical properties of sodium lead borate glasses. Journal of Advanced Ceramics 3(2):155–164. https://doi.org/10.1007/s40145-014-0107-z
37. Singh DP, Pal Singh G (2013) Conversion of covalent to ionic behavior of Fe_2O_3–CeO_2–PbO–B_2O_3 glasses for ionic and photonic application. J Alloys Compd 546:224–228. https://doi.org/10.1016/j.jallcom.2012.08.105
38. Duffy JA (2006) Ionic−covalent character of metal and nonmetal oxides. J Phys Chem A 110(49):13245–13248. https://doi.org/10.1021/jp063846j
39. Khater GA, Nabawy BS, Kang J, Yue Y, Mahmoud MA (2020) Magnetic and electrical properties of glass and glass-ceramics based on weathered basalt. Silicon. 12:2921–2940. https://doi.org/10.1007/s12633-020-00391-8
40. Kashif I, Soliman AA, Sakr EM, Ratep A (2013) XRD and FTIR studies the effect of heat treatment and doping the transition metal oxide on $LiNbO_3$ and $LiNb_3O_8$ nano-crystallite phases in lithium borate glass system. Spectrochim Acta A Mol Biomol Spectrosc 113:15–21. https://doi.org/10.1016/j.saa.2013.04.084
41. Kang J, Wang J, Cheng J, Yuan J, Hou Y, Qian S (2017) Crystallization behavior and properties of CaO-MgO-Al_2O_3-SiO_2 glass-ceramics synthesized from granite wastes. J Non-Cryst Solids 457:111–115. https://doi.org/10.1016/j.jnoncrysol.2016.11.030
42. Shaaban KS, Yousef ES, Abdel Wahab EA, Shaaban ER, Mahmoud SA (2020) Investigation of crystallization and mechanical characteristics of glass and glass-ceramic with the compositions $x$$Fe_2O_3-35SiO_2-35B_2O_3-10Al_2O_3$-(20–$x$) Na_2O. J of Materi Eng and Perform 29:4549–4558. https://doi.org/10.1007/s11665-020-04969-6
43. El-Rehim AFA, Shaaban KS, Zahran HY et al (2020) Structural and mechanical properties of Lithium bismuth borate glasses containing molybdenum (LBBM) together with their glass–ceramics. J Inorg Organomet Polym. https://doi.org/10.1007/s10904-020-01708-1
44. Syam Prasad N, Varma KB (2002) Nanocrystallization of $SrBi_2Nb_2O_9$ from glasses in the system $Li_2B_4O_7$-SrO-Bi_2O_3-Nb_2O_5. Mater Sci Eng B 90(3):246–253. https://doi.org/10.1016/s0921-5107(01)00919-9
45. Kamitsos EI, Patsis AP, Karakassides MA, Chryssikos GD (1990) Infrared reflectance spectra of lithium borate glasses. J Non-Cryst Solids 126(1–2):52–67. https://doi.org/10.1016/0022-3093(90)91023-k
46. Kavaz E, Yorgun NY (2018) Gamma ray buildup factors of lithium borate glasses doped with minerals. J Alloys Compd 752:61–67. https://doi.org/10.1016/j.ceramint.2019.05.028